

Efficient Operator Selection and Warm-Start Strategy for Excitations in Variational Quantum Eigensolvers

Max Haas^{1†}, Thierry N. Kaldenbach¹, Thomas Hammerschmidt² and Daniel Barragan-Yani¹

¹German Aerospace Center (DLR), Institute for Frontier Materials on Earth and in Space, Cologne, Germany

² ICAMS, Ruhr University Bochum, Bochum, Germany

We present a novel approach for efficient preparation of electronic ground states, leveraging the optimizer ExcitationSolve [Jäger et al., *Comm. Phys.* (2025)] and established variational quantum eigensolver-based operator selection methods, such as Energy Sorting. By combining these tools, we demonstrate a computationally efficient protocol that enables the construction of an approximate ground state from a unitary coupled cluster ansatz via a single sweep over the operator pool. Utilizing efficient classical pre-processing to select the majority of relevant operators, this approach reduces the computational complexity associated with traditional optimization methods. Furthermore, we show that this method can be seamlessly integrated with one-variational-parameter couple exchange operators, thereby further reducing the number of required CNOT operations. Overall, we empirically observe a quadratic convergence speedup beyond state-of-the-art methods, advancing the realization of quantum advantage in quantum chemistry.

1 Introduction

The variational quantum eigensolver (VQE) [1] has emerged as a paradigmatic approach to solve the ground-state problem in quantum many-body systems. This hybrid algorithm, which combines the computational power of both quantum and classical computers, has been subject to intense scrutiny and debate over the past decade [2–4]. Despite its promise, VQE is hampered by several fundamental challenges that hinder its ability to achieve quantum advantage [5].

One of the primary obstacles to overcoming this limitation is the phenomenon of barren plateaus, where the algorithm fails to converge due to exponentially vanishing gradients of the loss function [5–9]. This can be attributed to the expo-

nential growth of the Hilbert space and the so-called curse of dimensionality. Furthermore, traditional ansätze such as the Unitary Coupled Cluster Singles Doubles (UCCSD) [10] ansatz suffer from polynomial circuit depth scaling with respect to the number of electrons, resulting in deep circuits that are difficult to implement on current noisy intermediate-scale quantum (NISQ) devices.

To address these challenges, researchers have been exploring novel strategies, including different ansatz designs [7, 11, 12], optimization techniques [13–16] and initialization strategies [17, 18]. One promising approach is the use of adaptive ansätze such as ADAPT-VQE [19–21], which employs an iterative process to add operators one by one from a pool of possible choices. However, this approach comes at the cost of high computational overhead,

[†]Corresponding author: max.haas@dlr.de

caused by the evaluation of an excessive number of quantum circuits during the selection process. Energy Sorting (ES) [22] offers a solution to mitigate this limitation by selecting multiple operators simultaneously. By ranking all operators based on their impact on the energy and appending them to the ansatz in order, ES reduces the computational overhead associated with sequential operator addition. Moreover, ES can be parallelized to multiple quantum processing units (QPUs), thereby offering potential speedup opportunities.

In this work, we build upon the idea of ES by combining it with the recently developed optimizer ExcitationSolve [16]. Since ExcitationSolve reconstructs the cost function for each parameter, it enables the direct optimization of parameters without gradient descent. This allows us to perform energy sorting “for free” in the first selection step. We demonstrate the efficacy of this approach using UCCSD ansätze for a range of molecules, from 4 to 20 qubits and compare its performance with fixed and adaptive ansätze in terms of operator count and evaluation requirements on the quantum computer. Our results show that we can select all relevant operators within a single operator selection step. As already mentioned in the original publication [22], the first selection process is classically simulable, leaving us with a fully classical method to construct and warm-start the VQE. Notably, this approach can be adapted to accommodate the recently introduced One Variational Parameter Couple Exchange Operators (OVP-CEO) [23]. By adopting an OVP-CEO pool, we can further reduce the circuit depth compared to traditional ADAPT-VQE, at the cost of a small computational overhead.

2 Background and Methodological developments

The idea of a unitary coupled cluster (UCC) approach reaches back to the eighties and there has been continuous research in the decades since its first mention [24–27]. In more recent years, the

UCC has been quite popular in the context of quantum computing [28], as it is well suited to be mapped to a quantum device due to its unitary nature and because it describes the physically correct states of material systems. The unitary coupled cluster operator can be defined as

$$U = e^{-i \sum_N \hat{T}_N}, \quad (1)$$

where $\hat{T}_N = \sum_j \theta_j G_j$ is the sum over generators of fermionic excitations of order N , which assume the structure

$$G = i(a_{q_1}^\dagger \dots a_{q_N}^\dagger a_{p_1} \dots a_{p_N} - \text{H.c.}) \quad (2)$$

The indices $p_1 \dots q_N$ ($q_1 \dots q_N$) denote the N occupied (virtual) orbitals that generator G acts on. Most commonly used is the so-called unitary coupled cluster singles doubles (UCCSD) in which this sum is truncated after the second order ($N = 1, 2$) of excitation. To map U to a quantum computer however, it must be simplified to not contain a sum in the exponential. This can be achieved by Trotterization [29, 30], where U is approximated as

$$U \approx \left(\prod_j e^{-i \frac{\theta_j}{\tau} G_j} \right)^\tau + \mathcal{O}\left(\frac{1}{\tau}\right), \quad (3)$$

where an increasing number of Trotter steps τ leads to better approximations. Commonly, Trotterization is held to one Trotter step ($\tau = 1$) to keep the required quantum resources to a minimum, which is a good approximation given that the optimal θ_j are typically small.

The variational quantum eigensolver (VQE) [1] then takes such a unitary

$$U(\theta) = \prod_j U_j(\theta_j) = \prod_j e^{-i \theta_j G_j}, \quad (4)$$

and optimizes the tunable parameters θ_i such that the energy

$$E_{\text{VQE}} = \langle \Psi_0 | U^\dagger(\theta) H U(\theta) | \Psi_0 \rangle \quad (5)$$

is minimized. In ADAPT-VQE [19], U is not fixed

to contain all excitations from the beginning, but they are iteratively selected from a pool of generators $O = \{G_1, G_2, \dots, G_M\}$ and appended to the ansatz one by one. This comes at the cost of additional measurements for the operator selection, but reduces the depth of the resulting circuit significantly. The energy sorting algorithm (ES) [22] then tries to mitigate this additional overhead by selecting multiple operators at a time.

2.1 Energy sorting with Excitation-Solve

The ES algorithm works by simultaneously selecting all operators U_j whose energy impact, $\Delta E_j = E_{\text{ref}} - E_j$, exceeds a predetermined threshold value ϵ_A . E_{ref} is the reference energy of the system before appending any operator and E_j is the energy after appending U_j to the ansatz and optimizing the corresponding parameter θ_j . The optimizer ExciationSolve [16] provides an efficient means of calculating these energy differences. By fully reconstructing the energy landscape of each operator, ExciationSolve can identify all operators fulfilling the condition with a single sweep over the operator pool, without requiring further optimization. Consequently, when employing Excitation-Solve, ES can be performed with no additional computational effort compared to a single adaptive step. When the threshold ϵ_A is set to 0, all

operators contributing to the system's energy are selected simultaneously. These operators can then be sorted by their impact and appended to the circuit. Moreover, ExcitationSolve also provides the optimal parameter value for each operator, enabling a warm start by initializing the parameters θ_i to finite values rather than the commonly chosen $\theta_i = 0$. The resulting ansatz can then be optimized like a fixed ansatz VQE, eliminating the need for subsequent operator selection. For linear systems like the LiH molecule, the ansatz only needs to be constructed once and can be reused for any bond lengths, because the dissociation length does not change which orbitals overlap and therefore the relevant operators remain the same. Examples are given in Supplementary Material C.

2.2 Energy sorting for OVP-CEOs

The ExciationSolve algorithm is applicable to any pool, $O = \{G_1, G_2, \dots, G_M\}$ comprised of generators G that satisfy the condition $G^3 = G$. A recently developed class of operators fulfilling this condition are one-variational-parameter couple exchange operators (OVP-CEOs) [23]; a formal proof of this relationship is provided in Supplementary Material A). The OVP-CEOs are given by

$$T_{\alpha_1\beta_1\alpha_2\beta_2}^{(\text{OVP-CEO},+)}(\theta) = \theta(T_{\alpha_1\beta_1 \rightarrow \alpha_2\beta_2}^{(\text{QE})} + T_{\alpha_2\beta_1 \rightarrow \alpha_1\beta_2}^{(\text{QE})}) \\ = \theta(Q_{\alpha_2}^\dagger Q_{\beta_2}^\dagger Q_{\alpha_1} Q_{\beta_1} + Q_{\alpha_1}^\dagger Q_{\beta_2}^\dagger Q_{\alpha_2} Q_{\beta_1}) - \text{H.c.}, \quad (6)$$

$$T_{\alpha_1\beta_1\alpha_2\beta_2}^{(\text{OVP-CEO},-)}(\theta) = \theta(T_{\alpha_1\beta_1 \rightarrow \alpha_2\beta_2}^{(\text{QE})} - T_{\alpha_2\beta_1 \rightarrow \alpha_1\beta_2}^{(\text{QE})}) \\ = \theta(Q_{\alpha_2}^\dagger Q_{\beta_2}^\dagger Q_{\alpha_1} Q_{\beta_1} - Q_{\alpha_1}^\dagger Q_{\beta_2}^\dagger Q_{\alpha_2} Q_{\beta_1}) - \text{H.c.}, \quad (7)$$

with the qubit creation- and annihilation operators

$$Q_i^\dagger = \frac{1}{2} (X_i - iY_i), \quad Q_i = \frac{1}{2} (X_i + iY_i). \quad (8)$$

Key to their functionality are the terms $Q_{\alpha_1}^\dagger Q_{\beta_2}^\dagger Q_{\alpha_2} Q_{\beta_1}$ and their Hermitian conjugates (H.c.), which mix the excitation on the α -orbital with the de-excitation on the β -orbital, and

vice versa. This mixing reduces the quantum cost of implementing each excitation operator from a count of 13 CNOT gates (for standard qubit excitations [31, 32]) to 9 CNOT gates with OVP-CEO $_{\pm}$ and a depth of 11 to 7.

However, application of ExcitationSolve to a pool of OVP-CEO $^{+}$ and OVP-CEO $^{-}$ operators presents two challenges. First, the resulting variational ansatz is twice as deep as necessary. This arises because both OVP-CEO $^{+}$ and OVP-CEO $^{-}$ act like a double excitation when applied to the HF state, leading to redundant selection of either both or neither operator. This negates the gate count reduction afforded by OVP-CEO $_{\pm}$, resulting in circuits even deeper than those employing a UCCSD pool. Restricting the pool to solely OVP-CEO $^{+}$ or OVP-CEO $^{-}$ operators is insufficient to reach the same convergence, as demonstrated in Section 3.3. Second, a naive selection of OVP-CEO $_{\pm}$ based on their impact on the HF state leads to an increased initial energy. This is attributed to the orbital mixing terms within the OVP-CEO formulation, which are inactive on the HF state due to the virtual nature of the orbitals involved. However, subsequent application of other OVP-CEO $_{\pm}$ that occupy these virtual orbitals introduces a non-zero contribution from the de-excitation terms. To address this, an additional selection step is implemented that, for each pair of OVP-CEO $^{+}$ or OVP-CEO $^{-}$ acting on the same orbitals, determines which operator will be appended to the ansatz. The algorithm initiates with the pure OVP-CEO $^{+}$ pool, and all relevant operators are selected using ExcitationSolve, but are not immediately appended to the ansatz. Instead, they are ordered according to their predicted impact on the Hartree-Fock (HF) state. Subsequently, for each operator a determination is made as to whether the OVP-CEO $^{+}$ or OVP-CEO $^{-}$ variant is more advantageous and the selected operator is then added to the ansatz. This process is repeated for each operator in the ordered list. For the initial operator selection, the

choice is arbitrary and a distinction only exists due to numerical inaccuracies, as both OVP-CEO $^{+}$ and OVP-CEO $^{-}$ exhibit the same energy impact on the HF state. However, for operators added subsequently, the state upon which they act is no longer the HF state, resulting in potentially significant differences in their energy contributions. In each case, the operator with the greater predicted impact was chosen.

2.3 Classical simulation of the operator selection

When building the ansatz using ES from either a UCC or OVP-CEO pool, a large part of the operator selection can be performed classically, saving valuable quantum resources and giving a warm-start to the quantum simulation.

When applying a UCC ansatz on the reference state obtained from Hartree-Fock theory, one typically starts by considering all spin-preserving double excitations from occupied to virtual orbitals. The contributions of higher-order excitations, i.e., triples or higher, can always be ruled out as the electronic structure Hamiltonian only entails quadratic and quartic fermionic terms and therefore cannot couple two classical states that differ by more than a double-excitation [33]. It is proven that single excitations cannot lower the energy when applied to the HF ground state as it is the classical state with the energy closest to the true ground state. Thus, having a single-excitation lowering the energy would imply the existence of a different classical state with lower energy than the HF state [33].

The selection of the double excitations (or OVP-CEO $_{\pm}$) with ES works by testing each operator individually for its energy impact on the HF state, as described in detail in Section 2.1. The states for which the energy must be determined are thus a classical state with exactly one double excitation on top. Such unitary double excitation then spans the subspace of the HF state and the double-excited state. By reducing the electronic structure Hamiltonian

$$\Delta E := \Delta E(\theta_{\max}) = \frac{1}{2} \left(h_{pp} + h_{qq} - h_{rr} - h_{ss} + \sqrt{(h_{pp} + h_{qq} - h_{rr} - h_{ss})^2 + \Re\{h_{pqrs}\}^2} \right), \quad (9)$$

with the optimal angle

$$\theta_{\max} = \frac{\pi}{4} - \frac{1}{2} \arctan \left(\frac{h_{pp} + h_{qq} - h_{rr} - h_{ss}}{\Re\{h_{pqrs}\}} \right). \quad (10)$$

Using these equations, one can classically compute the energy impact of each double excitation and the warm start parameters. The action of the double excitation on the reference state can be reduced from eight Pauli rotations to a single one of the type $\exp(i\theta X_p X_q X_r Y_s)$. This can serve as a helpful circuit optimization technique to assemble the beginning of the circuit, as it has been demonstrated in Ref. [16]. For a rigorous proof of the energy impact and circuit simplifications, refer to Supplementary Material B.

After the first layer of double excitations, the state against which all other orders of excitations are tested is no longer a classical state. The presented formulas and circuits then no longer hold and the operator selection itself requires the quantum device.

Last, it is worth highlighting that if the reference state is obtained from Kohn-Sham theory, as observed in UCC-based post-DFT calculations [34, 35], single excitations can potentially lower the energy compared to the reference state. For that case, we also provide analytical formulas and circuit simplifications in Supplementary Material B.

2.4 Higher order excitations

When simulating molecules using a UCCSD ansatz, an inverse relation exists between the size of the simulated system and the precision of the converged energy obtained with all optimizers employed. For H_2 (4 qubits) most optimizers achieve an energy value that is closer than 1×10^{-13} Ha from the FCI solution, while for LiH (12 qubits), convergence plateaus at 1×10^{-5} Ha and for H_2O (14 qubits) at 1×10^{-4} Ha. Therefore, to achieve

a minimum precision of 1×10^{-3} Ha to the FCI solution (often referred to as chemical accuracy), for larger molecules the ansatz must be expanded to include higher order excitations to improve convergence [36]. Fortunately all fermionic or qubit excitation operators of any order satisfy the necessary condition of $G^3 = G$, rendering them compatible with ExcitationSolve [16]. However, analogous to single excitations, they cannot improve upon the HF state [33] and must therefore be selected after the double excitations have been appended to the ansatz. Their selection can therefore not be simulated efficiently classically as the reference state is no longer a classical state. Section 3.2 explores the convergence behavior when utilizing triple excitations for the example molecule LiH .

3 Results

3.1 Energy sorting using the UCCSD pool

Starting from a UCCSD pool of operators, an ansatz is constructed as explained in Section 2.1. The initial state is chosen to be the HF state and ϵ_A was set to 10^{-13} Ha to avoid the inclusion of contributions arising from numerical imprecision. Given that single excitations cannot lower the energy in a HF state [33], a sequential approach was adopted; relevant double excitations were initially identified and appended to the ansatz, followed by the selection and inclusion of single excitations. The selection of the double excitations can efficiently be performed on a classical computer as explained in Section 2.3, while the selection of the

single excitations and the following optimization have to be performed on a quantum device. In this case the quantum device is simulated by a noiseless state-vector simulator provided by the TenCirChem package [37]. Finding the optimal parameter value for a single operator U_j using ExcitationSolve requires the evaluation of the cost function Equation (5) at four different values of θ_j , which will be referred to as energy evaluations in the following text and figures.

The efficacy of this algorithm, coupled with an EnergySorting strategy (ExcitationSolve + ES), was evaluated for the molecules H_2 , H_3^+ , He_2 , OH^- , LiH , H_6 , H_2O , BeH_2 , NH_3 , BH_3 , CH_4 and C_2 , each modeled in their respective equilibrium geometry as given in the datasets [38–49]. The convergence behavior of ExcitationSolve + ES was benchmarked against the original ADAPT-VQE algorithm, and adaptive ExcitationSolve without ES. For NH_3 , BH_3 , CH_4 and C_2 it was not feasible to simulate ADAPT-VQE (yellow) due to its high computational runtime, for C_2 even adaptive ExcitationSolve was too costly.

In Figure 1 the convergence profiles of the different studied algorithms are presented. All curves utilize a dual-color scheme. Lighter shades indicate computational resources dedicated to operator selection, while darker shades represent resources allocated to variational quantum eigensolver (VQE) optimization. The results demonstrate that naive adaptive ExcitationSolve is dominated by the operator selection process. In contrast, the ES strategy enables operator selection in a single sweep, followed by a limited number of VQE optimization iterations. Following this initial construction, a final screening process verifies the absence of additional operators exceeding the E_{th} threshold. Consequently, the combination of ES and ExcitationSolve facilitates the construction of a compact ansatz comprised solely of operators contributing significantly to the ground state, and provides a warm-start to the optimization process by initializing each operator with its optimal parameter θ_j relative to the initial state.

Another trend is visible in Figure 1: for LiH with an operator pool of 92 operators ExcitationSolve + ES requires about 10^{-1} of the resources of pure ExcitationSolve, while for CH_4 with a pool size of 804 the cost is reduced by a factor of 10^{-2} . Figure 2 formalizes this trend and makes it clearly visible. Here the number of evaluations required to reach convergence is plotted over the respective pool size for each molecule on a log-log scale. Indeed, the computational resources required to run the VQE grows exponentially with the number of operators in the UCC pool for all methods. While using ExcitationSolve in a classical adapt-VQE setting gives a constant speed-up over ADAPT-VQE using GD as suggested in [16], using ExcitationSolve + ES even reduces the exponent significantly. An unweighted linear fit to the log-log data is used as guide to the eye. The slope is reduced approximately by a factor of 2 for ExcitationSolve + ES compared to both GD + gradient selection and Exc.Solve + Exc.Solve selection, so the speed-up is quadratic in the pool size.

ExcSolve + ES can be viewed as a method to efficiently construct a fixed ansatz based on a UCC pool, which removes all irrelevant operators from the ansatz and warm starts the simulation. Figure 3 compares the convergence of the ExcSolve + ES algorithm to a fixed UCCSD ansatz for the LiH molecule. The Exc.Solve + ES approach incurs an initial computational cost associated with operator selection, while the fixed ansatz immediately starts its optimization. However, the substantial number of operators within the fixed ansatz (96 for LiH), many of which exhibit minimal or no impact at all, significantly slows down the optimization process and leads to plateaus in the optimization curve. Once constructed, the ansatz generated by ES contains fewer operators (34 for LiH), making it more shallow and converging rapidly, outperforming the fixed UCCSD ansatz.

3.2 Higher order excitations

As the number of electrons in the systems studied in Figure 1 increases, the convergence of the

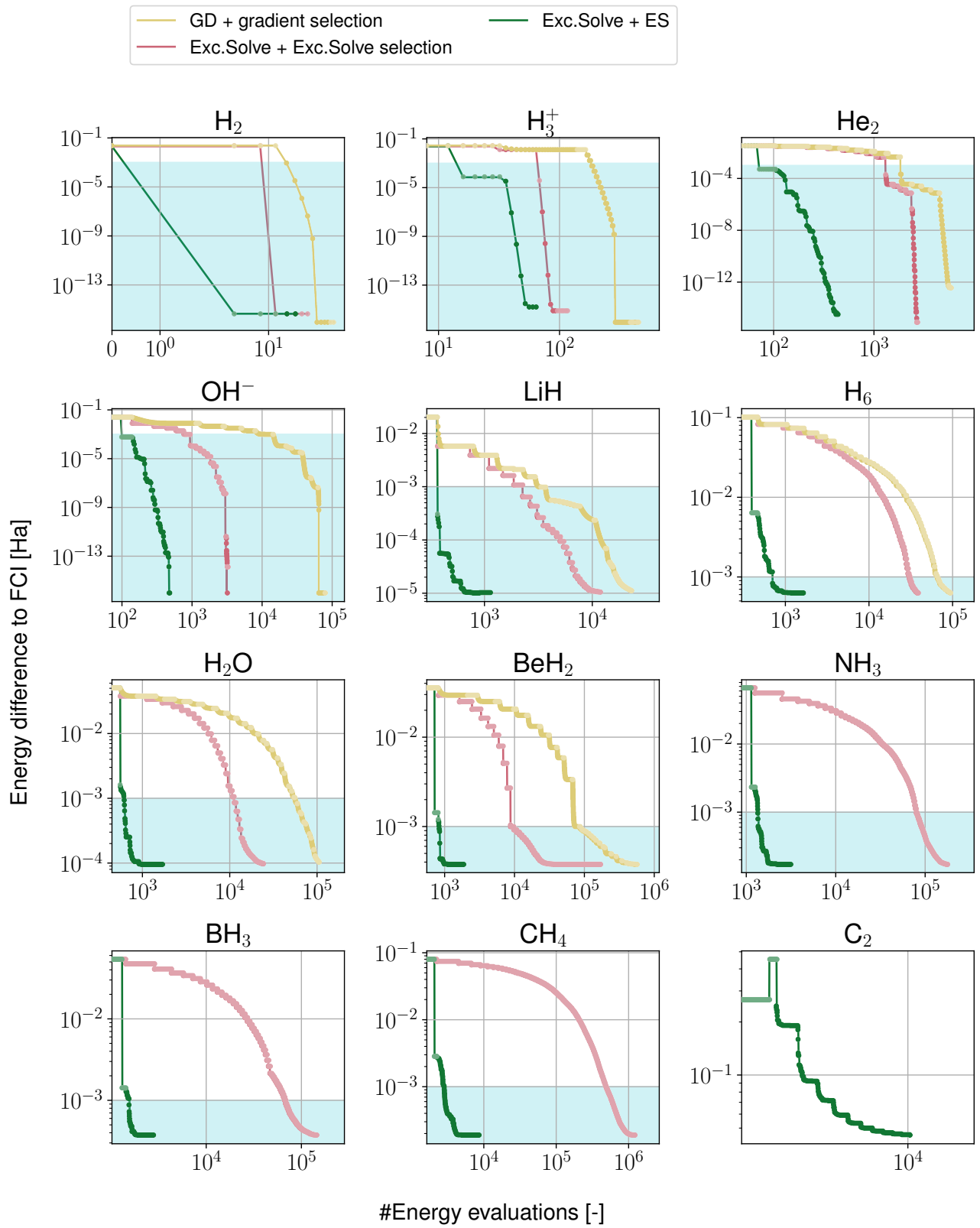


Figure 1: Comparison of ExcitationSolve + ES (green) to ADAPT VQE (yellow), naive adaptive ExcitationSolve (red), and a fixed ansatz UCCSD optimization (blue). Lighter colors signal quantum resources spent on operator selection, darker colors mean quantum resources spent on VQE optimization. The light blue area marks chemical accuracy.

Convergence vs. system size

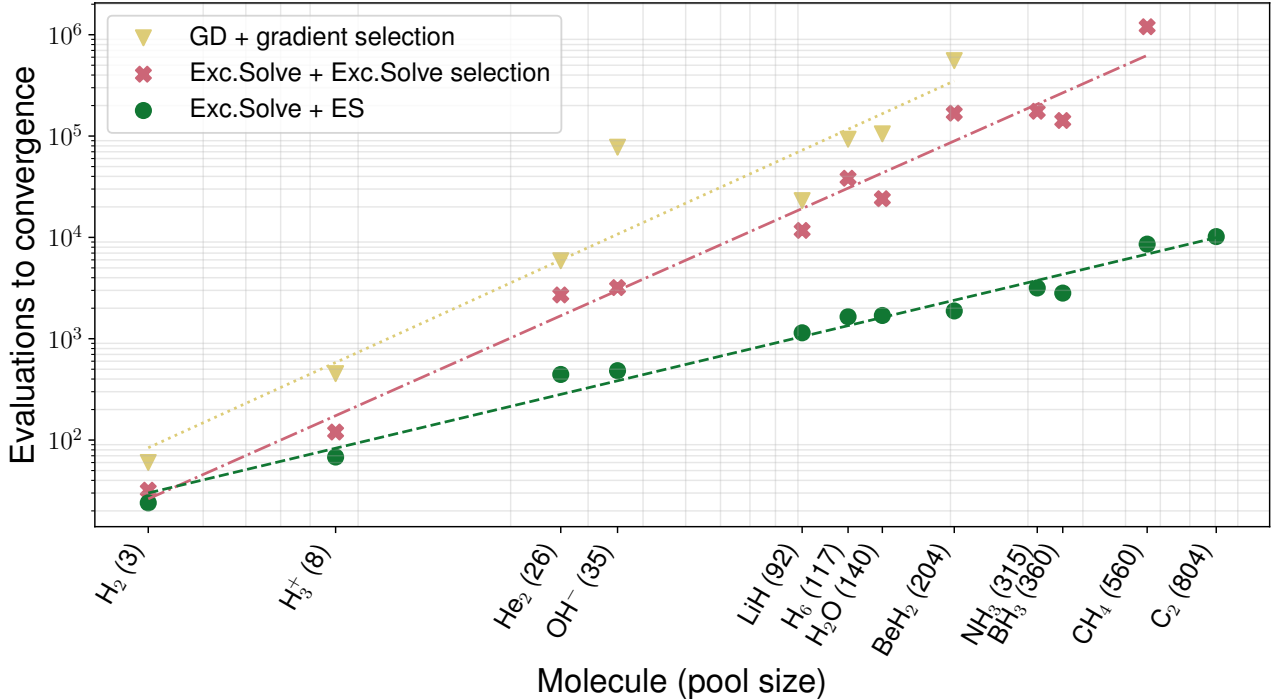


Figure 2: Evaluations to convergence over pool size on log-log scale, comparing ExcitationSolve + ES (green) to ADAPT VQE (yellow) and adaptive ExcitationSolve (red). An unweighted linear fit to the log-log data is used as guide to the eye. As the pool size grows, the number of evaluations required on the QC grows exponentially in all cases, but the exponent when using ExcitationSolve + ES is reduced significantly.

VQE is increasingly limited by the order of excitations permitted in the ansatz. While a precision of 10^{-15} Ha can be achieved for H_2 , calculations for H_2O are limited to 10^{-4} Ha, and for C_2 the results no longer even reach chemical accuracy. Consequently, scaling up simulations requires not only accounting for the $\mathcal{O}(n^4)$ growth in the number of double excitations, with n being the number of electrons in the system, but also incorporating higher-order excitations to attain the desired precision. Converging a VQE with a fixed ansatz entailing triple-, or higher order excitations quickly becomes computationally intractable due to the rapid increase in circuit depth with each added order of operator, i.e., the number of Pauli terms in the excitation generators grows exponentially with the order of the excitations.

Fortunately, any order of fermionic or qubit operator can be treated with ExcitationSolve, enabling the ES protocol to include only the necessary operators in the ansatz. Figure 4 demonstrates the

improved convergence achieved with triple excitations for the LiH molecule. The process starts again by selecting only double excitations, as these are the only operators that directly impact the HF state. Once the relevant double excitations have been appended to the ansatz, single and triple excitations are selected. This selection process is evident in the extended plateau observed around 500 evaluations in Figure 4. The resulting ansatz is then optimized using ExcitationSolve. This approach achieves a precision more than two orders of magnitude better than using only double excitations, at the cost of approximately three times the number of evaluations and the inclusion of 10 triple excitations.

3.3 Energy sorting using OVP-CEO_s

The OVP-CEO_s were implemented according to ref. [23]. An operator pool, O_{CEO} , was then constructed comprising all OVP-CEO⁺ and OVP-CEO⁻ operators, in addition to single excitations.

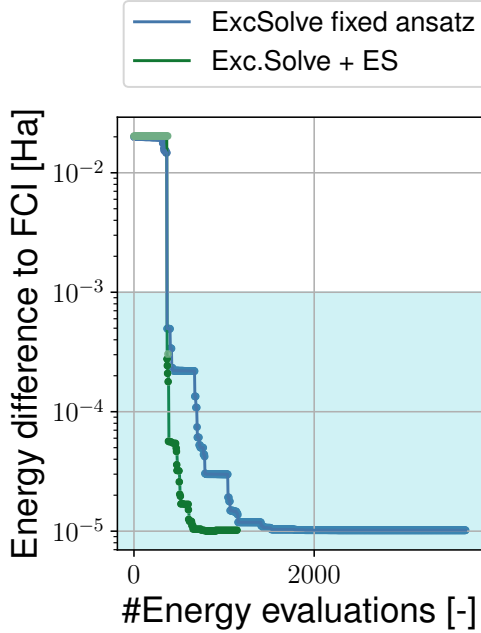


Figure 3: Fixed ansatz (blue) convergence compared to ExcitationSolve + ES (green) for the LiI molecule. Even though the convergence process begins earlier for the fixed ansatz, the optimization using ES is faster, because all unnecessary operators are removed from the ansatz. The light blue area marks chemical accuracy.

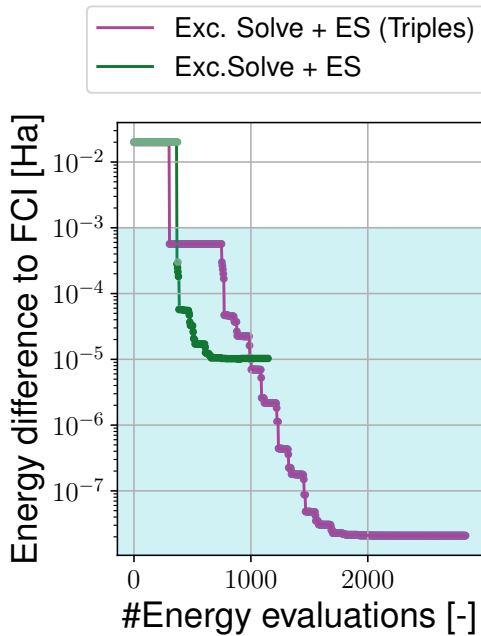


Figure 4: ExcitationSolve and Energy Sorting for a UCCSDT pool (purple) for a LiH molecule compared to a UCCSD pool (green). First double excitations are appended to the ansatz, then singles and lastly triples, followed by the optimization of the complete circuit. The light blue area marks chemical accuracy.

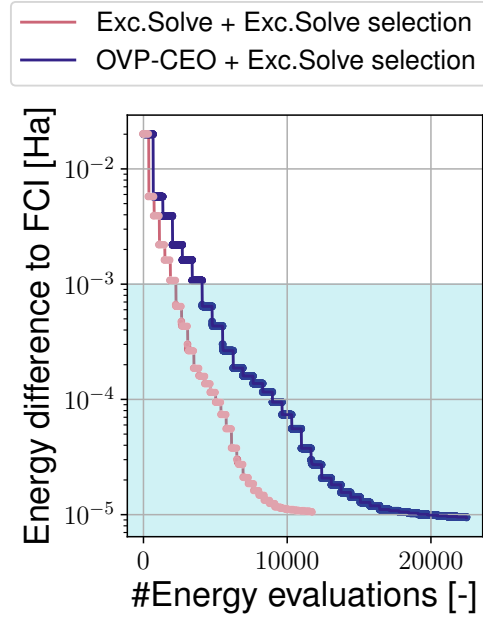


Figure 5: Adaptive optimization of an OVP-CEO pool (blue) compared to a UCCSD pool (red) of LiH. Convergence is reached with the same number of operators, but for OVP-CEO₊s twice as many evaluations are needed due to the increased pool size. The light blue area marks chemical accuracy.

Given that one OVP-CEO₊ and one OVP-CEO₋ operator exist for each double excitation within the UCCSD pool, the size of the O_{CEO} pool is approximately double that of the UCCSD pool. Operator selection and ansatz optimization were performed using the ExcitationSolve algorithm.

Figure 5 shows the convergence of an adaptive ansatz utilizing OVP-CEO₊s, compared to that employing the UCCSD pool [42], for the LiH molecule. The optimizer converges to the same ground state energy with the same number of operators. However, the larger pool size necessitates approximately twice the number of energy evaluations, increasing the computational cost of operator selection. This represents a trade-off between the depth of the resulting quantum circuit and the number of evaluations required.

ExcitationSolve was then applied to a pool consisting solely of OVP-CEO₊ operators and the convergence behavior was compared to that of a pool of qubit excitation operators, see Figure 6. The resulting ansatz comprised of OVP-CEO₊ op-

erators exhibits insufficient expressivity to achieve the same level of precision upon convergence. To incorporate OVP-CEO[−] operators into the ansatz without doubling the circuit depth, an additional operator selection process was implemented as discussed in Section 2.2.

This additional selection process increases the number of evaluations performed on the quantum computer, but enables the effective combination of ExcitationSolve with OVP-CEO[−]s. Comparing the convergence behaviors presented in Figure 6, the use of OVP-CEO[−]s with this selection criterion is found to be less than a factor of two slower than using excitation operators, while retaining the advantage of reduced circuit complexity – decreasing the number of CNOT gates per operator from 13 to 9, and depth from 11 to 7. For currently available NISQ hardware, where circuit depth is the limiting factor, this represents a favorable trade-off.

4 Discussion

In this study, we employed the ExcitationSolve optimizer in conjunction with EnergySorting (ES) to develop an efficient hybrid method for constructing ansätze in quantum computing. Specifically, we combined the shallow circuits of ADAPT-VQE with the limited number of optimization steps from fixed ansatz optimization. By leveraging ES, which enables the computation of the change in energy caused by each operator within a single sweep over the operator pool, this approach eliminates the need for repeated evaluations of individual operators and significantly reduces the computational complexity associated with optimizing the ansatz. We even derived an analytical equation, which allows operator selection directly from Hamiltonian matrix elements. This approach enables the construction of an ansatz consisting solely of the most relevant operators, mirroring the strategy employed in ADAPT-VQE, but with reduced computational overhead. We demonstrated the efficacy of our

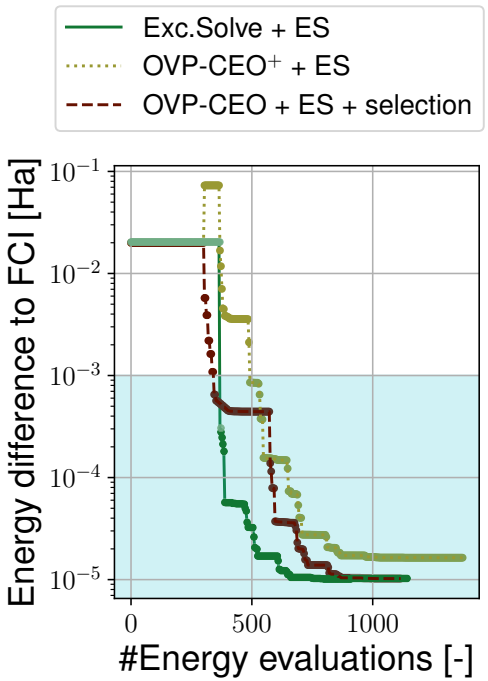


Figure 6: Combination of ES and OVP-CEO[−]s. The light green curve shows the problems of a naive combination of a pool consisting of only OVP-CEO⁺. With an additional selection step (brown) the performance can be improved to converge to the same energy as with the excitation operators (dark green). The dark green curve is the same as in Figure 6 and serves as a reference. The light blue area marks chemical accuracy.

method on twelve benchmark molecules, achieving a quadratic speed-up compared to the original ADAPT-VQE while maintaining equivalent circuit depth. We further refined our approach by adapting it to accommodate OVP-CEO[−]s, a novel class of operators that can reduce circuit depth at the cost of increased operator pool size. This trade-off is particularly relevant in the context of noisy intermediate-scale quantum (NISQ) hardware, where circuit depth limitations are a significant challenge. Our method’s performance was evaluated on the example of LiH, yielding improved computational efficiency with minimal loss in precision.

The knowledge of all relevant operators before the ansatz construction leaves potential for further reduction of the circuit depth as algorithms like Tetris-ADAPT [11] could be employed to stack the operators in the most favorable way.

As our method reduces compute times from days down to minutes (as in the example of CH₄), such a speed-up makes the out-of-the-box simulation of larger molecules feasible. While larger molecular simulations up to 28 qubits have already been demonstrated [50, 51], most of recent literature focuses on systems up to 12 qubits [33, 52, 53]. We hope that our work contributes to increasing the size and variety of molecules studied in the future.

While our methodology has been specifically tailored for VQE, we envision its broader applicability to other fields of material research as a pre-processing step, to make computationally expensive methods such as Quantum Monte Carlo (QMC), Quantum Phase Estimation (QPE) or Quantum Subspace Expansion (QSE) more feasible as most of them strongly depend on an initial state that is close to the actual ground state. And even beyond molecules or quantum chemistry the classical pre-processing can be useful, for example in Hamiltonian variational methods [54], as it can be applied to any rotation- or excitation based ansätze.

tationSolve and Energy Sorting methods and their application to OVP-CEO operators. The listed inventors are identical to the authors of this work. The application number is DE 10 2025 132 756.4, with the German title “Verfahren zur Bestimmung von Energien und Energiezuständen eines fermionischen Systems”. The authors declare no other financial or non-financial competing interests.

Author contributions

M.H. led the project, performed all coding and data analysis, and wrote the main draft of the manuscript. T.N.K conducted the theoretical proofs and contributed to the writing and revision of the manuscript. D.B.Y and T.H. contributed to the conceptual development of the work and provided guidance and feedback throughout the research and writing process. All authors reviewed and approved the final manuscript.

Acknowledgments

The authors would like to thank Erik Schultheis for kindly providing code that supported part of the implementation used in this work. M.H. acknowledges funding by the DLR Quantum Fellowship Program. This project was made possible by the DLR Quantum Computing Initiative and the Federal Ministry for Economic Affairs and Climate Action; <https://qci.dlr.de/quanticom>.

Conflicting interests

A patent application filed by the German Aerospace Center (Deutsches Zentrum für Luft- und Raumfahrt e.V., DLR), currently pending with the German Patent and Trade Mark Office (Deutsches Patent- und Markenamt, DPMA), covers aspects of this work. It specifically includes, but is not limited to, the combination of the Exc-

References

[1] Alberto Peruzzo et al. “A variational eigenvalue solver on a photonic quantum processor”. In: *Nature Communications* 5.1 (2014), p. 4213. ISSN: 2041-1723. DOI: [10.1038/ncomms5213](https://doi.org/10.1038/ncomms5213).

[2] M. Cerezo et al. “Variational quantum algorithms”. In: *Nature Reviews Physics* 3.9 (2021), pp. 625–644. ISSN: 2522-5820. DOI: [10.1038/s42254-021-00348-9](https://doi.org/10.1038/s42254-021-00348-9).

[3] Suguru Endo et al. “Hybrid Quantum-Classical Algorithms and Quantum Error Mitigation”. In: *Journal of the Physical Society of Japan* 90.3 (2021), p. 032001. DOI: [10.7566/JPSJ.90.032001](https://doi.org/10.7566/JPSJ.90.032001).

[4] Jérôme F. Gonthier et al. “Measurements as a roadblock to near-term practical quantum advantage in chemistry: Resource analysis”. In: *Phys. Rev. Res.* 4 (3) (2022), p. 033154. DOI: [10.1103/PhysRevResearch.4.033154](https://doi.org/10.1103/PhysRevResearch.4.033154).

[5] M. Cerezo et al. “Does provable absence of barren plateaus imply classical simulability?” In: *Nature Communications* 16.1 (2025), p. 7907. ISSN: 2041-1723. DOI: [10.1038/s41467-025-63099-6](https://doi.org/10.1038/s41467-025-63099-6).

[6] Jack Cunningham and Jun Zhuang. “Investigating and mitigating barren plateaus in variational quantum circuits: a survey”. In: *Quantum Information Processing* 24.2 (2025), p. 48. ISSN: 1573-1332. DOI: [10.1007/s11128-025-04665-1](https://doi.org/10.1007/s11128-025-04665-1).

[7] Xia Liu et al. “Mitigating Barren Plateaus of Variational Quantum Eigensolvers”. In: *IEEE Transactions on Quantum Engineering* 5.3103719 (2024). DOI: [10.1109/TQE.2024.3383050](https://doi.org/10.1109/TQE.2024.3383050).

[8] Samson Wang et al. “Noise-induced barren plateaus in variational quantum algorithms”. In: *Nature Communications* 12.1 (2021), p. 6961. ISSN: 2041-1723. DOI: [10.1038/s41467-021-27045-6](https://doi.org/10.1038/s41467-021-27045-6).

[9] A V Uvarov and J D Biamonte. “On barren plateaus and cost function locality in variational quantum algorithms”. In: *Journal of Physics A: Mathematical and Theoretical* 54.24 (2021), p. 245301. DOI: [10.1088/1751-8121/abfac7](https://doi.org/10.1088/1751-8121/abfac7).

[10] Rongxin Xia and Sabre Kais. “Qubit coupled cluster singles and doubles variational quantum eigensolver ansatz for electronic structure calculations”. In: *Quantum Science and Technology* 6.1 (2020), p. 015001. DOI: [10.1088/2058-9565/abbc74](https://doi.org/10.1088/2058-9565/abbc74).

[11] Panagiotis G. Anastasiou et al. “TETRIS-ADAPT-VQE: An adaptive algorithm that yields shallower, denser circuit Ansätze”. In: *Phys. Rev. Res.* 6 (1) (2024), p. 013254. DOI: [10.1103/PhysRevResearch.6.013254](https://doi.org/10.1103/PhysRevResearch.6.013254).

[12] Chae-Yeun Park, Minhyeok Kang, and Joonsuk Huh. “Hardware-efficient ansatz without barren plateaus in any depth”. In: *arXiv* 2403.04844 (2024). DOI: <https://doi.org/10.48550/arXiv.2403.04844>.

[13] Ken M. Nakanishi, Keisuke Fujii, and Synge Todo. “Sequential Minimal Optimization for Quantum-Classical Hybrid Algorithms”. In: *Physical Review Research* 2.4 (2020), p. 043158. ISSN: 2643-1564. DOI: [10.1103/PhysRevResearch.2.043158](https://doi.org/10.1103/PhysRevResearch.2.043158).

[14] Mateusz Ostaszewski, Edward Grant, and Marcello Benedetti. “Structure optimization for parameterized quantum circuits”. In: *Quantum* 5 (2021), p. 391. ISSN: 2521-327X. DOI: [10.22331/q-2021-01-28-391](https://doi.org/10.22331/q-2021-01-28-391).

[15] Jakob S. Kottmann, Abhinav Anand, and Alán Aspuru-Guzik. “A feasible approach for automatically differentiable unitary coupled-cluster on quantum computers”. In: *Chem. Sci.* 12 (10) (2021), pp. 3497–3508. DOI: [10.1039/DOSC06627C](https://doi.org/10.1039/DOSC06627C).

[16] Jonas Jäger et al. “Fast gradient-free optimization of excitations in variational quantum eigensolvers”. In: *Communications Physics* 8.1 (2025), p. 418. ISSN: 2399-3650. DOI: [10.1038/s42005-025-02375-9](https://doi.org/10.1038/s42005-025-02375-9).

[17] Ricard Puig et al. “Variational Quantum Simulation: A Case Study for Understanding Warm Starts”. In: *PRX Quantum* 6 (1) (2025), p. 010317. DOI: [10.1103/PRXQuantum.6.010317](https://doi.org/10.1103/PRXQuantum.6.010317).

[18] Felix Truger et al. “Warm-Starting the VQE with Approximate Complex Amplitude Encoding”. In: *arXiv* 2402.17378 (2024). DOI: <https://doi.org/10.5220/0013513400004525>.

[19] Harper R. Grimsley et al. “An adaptive variational algorithm for exact molecular simulations on a quantum computer”. In: *Nature Communications* 10.1 (2019), p. 3007. ISSN: 2041-1723. DOI: [10.1038/s41467-019-10988-2](https://doi.org/10.1038/s41467-019-10988-2).

[20] Ho Lun Tang et al. “Qubit-ADAPT-VQE: An Adaptive Algorithm for Constructing Hardware-Efficient Ansätze on a Quantum Processor”. In: *PRX Quantum* 2 (2) (2021), p. 020310. DOI: [10.1103/PRXQuantum.2.020310](https://doi.org/10.1103/PRXQuantum.2.020310).

[21] Harper R. Grimsley et al. “Adaptive, problem-tailored variational quantum eigensolver mitigates rough parameter landscapes and barren plateaus”. In: *npj Quantum Information* 9.1 (2023), p. 19. ISSN: 2056-6387. DOI: [10.1038/s41534-023-00681-0](https://doi.org/10.1038/s41534-023-00681-0).

[22] Yi Fan et al. “Circuit-Depth Reduction of Unitary-Coupled-Cluster Ansatz by Energy Sorting”. In: *The Journal of Physical Chemistry Letters* 14.43 (2023). PMID: 37862387, pp. 9596–9603. DOI: [10.1021/acs.jpclett.3c01804](https://doi.org/10.1021/acs.jpclett.3c01804).

[23] Mafalda Ramôa et al. “Reducing the resources required by adapt-vqe using coupled exchange operators and improved subroutines”. In: *npj Quantum Information* 11.1 (2025), pp. 1–19. DOI: [10.1038/s41534-025-01039-4](https://doi.org/10.1038/s41534-025-01039-4).

[24] Werner Kutzelnigg. “Quantum chemistry in Fock space. I. The universal wave and energy operators”. In: *The Journal of Chemical Physics* 77.6 (1982), pp. 3081–3097. ISSN: 0021-9606. DOI: [10.1063/1.444231](https://doi.org/10.1063/1.444231).

[25] Werner Kutzelnigg and Sigurd Koch. “Quantum chemistry in Fock space. II. Effective Hamiltonians in Fock space”. In: *The Journal of Chemical Physics* 79.9 (1983), pp. 4315–4335. ISSN: 0021-9606. DOI: [10.1063/1.446313](https://doi.org/10.1063/1.446313).

[26] Werner Kutzelnigg. “Quantum chemistry in Fock space. III. Particle-hole formalism”. In: *The Journal of Chemical Physics* 80.2 (1984), pp. 822–830. ISSN: 0021-9606. DOI: [10.1063/1.446736](https://doi.org/10.1063/1.446736).

[27] Rodney J. Bartlett and Jozef Noga. “The expectation value coupled-cluster method and analytical energy derivatives”. In: *Chemical Physics Letters* 150.1 (1988), pp. 29–36. ISSN: 0009-2614. DOI: [https://doi.org/10.1016/0009-2614\(88\)80392-0](https://doi.org/10.1016/0009-2614(88)80392-0).

[28] Abhinav Anand et al. “A quantum computing view on unitary coupled cluster theory”. In: *Chem. Soc. Rev.* 51 (5) (2022), pp. 1659–1684. DOI: [10.1039/D1CS00932J](https://doi.org/10.1039/D1CS00932J).

[29] H. F. Trotter. “On the Product of Semigroups of Operators”. In: *Proceedings of the American Mathematical Society* 10.4 (1959), pp. 545–551. ISSN: 00029939, 10886826. DOI: <https://doi.org/10.1090/S0002-9939-1959-0108732-6>.

[30] Masuo Suzuki. “Generalized Trotter’s formula and systematic approximants of exponential operators and inner derivations with applications to many-body problems”. In: *Communications in Mathematical Physics* 51.2 (1976), pp. 183–190. ISSN: 1432-0916. DOI: [10.1007/BF01609348](https://doi.org/10.1007/BF01609348).

[31] Yordan S. Yordanov, David R. M. Arvidsson-Shukur, and Crispin H. W. Barnes. “Efficient quantum circuits for quantum computational chemistry”. In: *Phys. Rev. A* 102 (6) (2020), p. 062612. DOI: [10.1103/PhysRevA.102.062612](https://doi.org/10.1103/PhysRevA.102.062612).

[32] Yordan S. Yordanov et al. “Qubit-excitation-based adaptive variational quantum eigensolver”. In: *Communications Physics* 4.1 (2021), p. 228. ISSN: 2399-3650. DOI: [10.1038/s42005-021-00730-0](https://doi.org/10.1038/s42005-021-00730-0).

[33] V. O. Shkolnikov et al. “Avoiding symmetry roadblocks and minimizing the measurement overhead of adaptive variational quantum eigensolvers”. In: *Quantum* 7 (2023), p. 1040. ISSN: 2521-327X. DOI: [10.22331/q-2023-06-12-1040](https://doi.org/10.22331/q-2023-06-12-1040).

[34] He Ma, Marco Govoni, and Giulia Galli. “Quantum simulations of materials on near-term quantum computers”. In: *npj Computational Materials* 6.1 (2020), p. 85. DOI: [10.1038/s41524-020-00353-z](https://doi.org/10.1038/s41524-020-00353-z).

[35] Erik Schultheis, Alexander Rehn, and Gabriel Breuil. “Many-body post-processing of density functional calculations using the variational quantum eigensolver for Bader charge analysis”. In: *arXiv* 2510.12887 (2025). DOI: <https://doi.org/10.48550/arXiv.2510.12887>.

[36] Mohammad Haidar et al. “Extension of the Trotterized Unitary Coupled Cluster to Triple Excitations”. In: *The Journal of Physical Chemistry A* 127.15 (2023), pp. 3543–3550. ISSN: 1089-5639. DOI: [10.1021/acs.jpca.3c01753](https://doi.org/10.1021/acs.jpca.3c01753).

[37] Weitang Li et al. “TenCirChem: An Efficient Quantum Computational Chemistry Package for the NISQ Era”. In: *Journal of Chemical Theory and Computation* 19.13 (2023), pp. 3966–3981. ISSN: 1549-9618. DOI: [10.1021/acs.jctc.3c00319](https://doi.org/10.1021/acs.jctc.3c00319).

[38] Utkarsh Azad and Stepan Fomichev. *PennyLane Quantum Chemistry Datasets*. <https://pennylane.ai/datasets/h2-molecule>. 2023.

[39] Utkarsh Azad and Stepan Fomichev. *PennyLane Quantum Chemistry Datasets*. <https://pennylane.ai/datasets/h3-plus-molecule>. 2023.

[40] Utkarsh Azad and Stepan Fomichev. *PennyLane Quantum Chemistry Datasets*. <https://pennylane.ai/datasets/he2-molecule>. 2023.

[41] Utkarsh Azad and Stepan Fomichev. *PennyLane Quantum Chemistry Datasets*. <https://pennylane.ai/datasets/oh-molecule>. 2023.

[42] Utkarsh Azad and Stepan Fomichev. *PennyLane Quantum Chemistry Datasets*. <https://pennylane.ai/datasets/lih-molecule>. 2023.

[43] Utkarsh Azad and Stepan Fomichev. *PennyLane Quantum Chemistry Datasets*. <https://pennylane.ai/datasets/h6-molecule>. 2023.

[44] Utkarsh Azad and Stepan Fomichev. *PennyLane Quantum Chemistry Datasets*. <https://pennylane.ai/datasets/h2o-molecule>. 2023.

[45] Utkarsh Azad and Stepan Fomichev. *PennyLane Quantum Chemistry Datasets*. <https://pennylane.ai/datasets/beh2-molecule>. 2023.

[46] Utkarsh Azad and Stepan Fomichev. *PennyLane Quantum Chemistry Datasets*. <https://pennylane.ai/datasets/nh3-molecule>. 2023.

[47] Utkarsh Azad and Stepan Fomichev. *PennyLane Quantum Chemistry Datasets*. <https://pennylane.ai/datasets/bh3-molecule>. 2023.

[48] Utkarsh Azad and Stepan Fomichev. *PennyLane Quantum Chemistry Datasets*. <https://pennylane.ai/datasets/ch4-molecule>. 2023.

[49] Utkarsh Azad and Stepan Fomichev. *PennyLane Quantum Chemistry Datasets*. <https://pennylane.ai/datasets/c2-molecule>. 2023.

[50] Changsu Cao et al. “Progress toward larger molecular simulation on a quantum computer: Simulating a system with up to 28 qubits accelerated by point-group symmetry”. In: *Phys. Rev. A* 105 (6) (2022), p. 062452. DOI: [10.1103/PhysRevA.105.062452](https://doi.org/10.1103/PhysRevA.105.062452).

[51] Palak Chawla et al. “Relativistic variational-quantum-eigensolver calculations of molecular electric dipole moments on quantum hardware”. In: *Phys. Rev. A* 111 (2) (2025), p. 022817. DOI: [10.1103/PhysRevA.111.022817](https://doi.org/10.1103/PhysRevA.111.022817).

[52] Palak Chawla et al. “Trapped ion quantum hardware demonstration of energy calculations using a multireference unitary coupled cluster ansatz: application to the BeH₂ insertion problem”. In: *The European Physical Journal Plus* 140.9 (2025), p. 924. ISSN: 2190-5444. DOI: [10.1140/epjp/s13360-025-06876-y](https://doi.org/10.1140/epjp/s13360-025-06876-y).

[53] Shaojun Guo et al. “Experimental quantum computational chemistry with optimized unitary coupled cluster ansatz”. In: *Nature Physics* 20.8 (2024), pp. 1240–1246. ISSN: 1745-2481. DOI: [10.1038/s41567-024-02530-z](https://doi.org/10.1038/s41567-024-02530-z).

[54] Dave Wecker, Matthew B. Hastings, and Matthias Troyer. “Progress towards practical quantum variational algorithms”. In: *Phys. Rev. A* 92 (4) (2015), p. 042303. DOI: [10.1103/PhysRevA.92.042303](https://doi.org/10.1103/PhysRevA.92.042303).

[55] Pascual Jordan and Eugene Paul Wigner. *Über das paulische Äquivalenzverbot*. Springer, 1993. ISBN: 978-3-662-02781-3. DOI: [10.1007/978-3-662-02781-3_9](https://doi.org/10.1007/978-3-662-02781-3_9).

A Proof that $G^3 = G$ holds for OVP-CEOs

ExcitationSolve requires unitary operators of the form

$$U(\theta) = \exp(-i\theta G), \quad (11)$$

with the Hermitian generator G fulfilling $G^3 = G$. The two possible OVP-CEO generators are given as

$$\begin{aligned} G_{\alpha_1\beta_1\alpha_2\beta_2}^{(\text{OVP-CEO},+)} &:= G_{\alpha_1\beta_1 \rightarrow \alpha_2\beta_2}^{(\text{QE})} + G_{\alpha_2\beta_1 \rightarrow \alpha_1\beta_2}^{(\text{QE})} \\ &= Q_{\alpha_2}^\dagger Q_{\beta_2}^\dagger Q_{\alpha_1} Q_{\beta_1} + Q_{\alpha_1}^\dagger Q_{\beta_2}^\dagger Q_{\alpha_2} Q_{\beta_1} - \text{H.c.} \\ &= \frac{1}{4}(X_{\alpha_1} X_{\beta_1} X_{\alpha_2} Y_{\beta_2} - X_{\alpha_1} X_{\beta_1} Y_{\alpha_2} X_{\beta_2} + Y_{\alpha_1} Y_{\beta_1} X_{\alpha_2} Y_{\beta_2} - Y_{\alpha_1} Y_{\beta_1} Y_{\alpha_2} X_{\beta_2}) \\ &= \frac{1}{4}X_{\alpha_1} X_{\beta_1} X_{\alpha_2} Y_{\beta_2} \cdot (I_{\alpha_1} I_{\beta_1} I_{\alpha_2} I_{\beta_2} - I_{\alpha_1} I_{\beta_1} Z_{\alpha_2} Z_{\beta_2} - Z_{\alpha_1} Z_{\beta_1} I_{\alpha_2} I_{\beta_2} + Z_{\alpha_1} Z_{\beta_1} Z_{\alpha_2} Z_{\beta_2}), \end{aligned} \quad (12)$$

$$\begin{aligned} G_{\alpha_1\beta_1\alpha_2\beta_2}^{(\text{OVP-CEO},-)} &:= G_{\alpha_1\beta_1 \rightarrow \alpha_2\beta_2}^{(\text{QE})} - G_{\alpha_2\beta_1 \rightarrow \alpha_1\beta_2}^{(\text{QE})} \\ &= Q_{\alpha_2}^\dagger Q_{\beta_2}^\dagger Q_{\alpha_1} Q_{\beta_1} - Q_{\alpha_1}^\dagger Q_{\beta_2}^\dagger Q_{\alpha_2} Q_{\beta_1} - \text{H.c.} \\ &= \frac{1}{4}(X_{\alpha_1} Y_{\beta_1} X_{\alpha_2} X_{\beta_2} - X_{\alpha_1} Y_{\beta_1} Y_{\alpha_2} Y_{\beta_2} + Y_{\alpha_1} X_{\beta_1} X_{\alpha_2} X_{\beta_2} - Y_{\alpha_1} X_{\beta_1} Y_{\alpha_2} Y_{\beta_2}) \\ &= \frac{1}{4}X_{\alpha_1} X_{\beta_1} X_{\alpha_2} Y_{\beta_2} \cdot (I_{\alpha_1} Z_{\beta_1} I_{\alpha_2} Z_{\beta_2} - I_{\alpha_1} Z_{\beta_1} Z_{\alpha_2} I_{\beta_2} - Z_{\alpha_1} I_{\beta_1} I_{\alpha_2} Z_{\beta_2} + Z_{\alpha_1} I_{\beta_1} Z_{\alpha_2} I_{\beta_2}), \end{aligned} \quad (13)$$

with the corresponding OVP-CEO unitaries defined as

$$U_{\alpha_1\beta_1\alpha_2\beta_2}^{(\text{OVP-CEO},\pm)}(\theta) := \exp\left(-i\theta G_{\alpha_1\beta_1\alpha_2\beta_2}^{(\text{OVP-CEO},\pm)}\right). \quad (14)$$

We now prove that the OVP-CEO generators indeed satisfy the requirement for ExcitationSolve, namely $G^3 = G$. We exemplify the proof at hand of G^+ , but the proof for G^- follows analogously. We begin with calculating $(G^+)^2$:

$$\begin{aligned} (G^+)^2 &= \left[\frac{1}{4}X_{\alpha_1} X_{\beta_1} X_{\alpha_2} Y_{\beta_2} \cdot (I_{\alpha_1} I_{\beta_1} I_{\alpha_2} I_{\beta_2} - I_{\alpha_1} I_{\beta_1} Z_{\alpha_2} Z_{\beta_2} - Z_{\alpha_1} Z_{\beta_1} I_{\alpha_2} I_{\beta_2} + Z_{\alpha_1} Z_{\beta_1} Z_{\alpha_2} Z_{\beta_2}) \right]^2 \\ &= \frac{1}{16}(X_{\alpha_1} X_{\beta_1} X_{\alpha_2} Y_{\beta_2})^2 \cdot (I_{\alpha_1} I_{\beta_1} I_{\alpha_2} I_{\beta_2} - I_{\alpha_1} I_{\beta_1} Z_{\alpha_2} Z_{\beta_2} - Z_{\alpha_1} Z_{\beta_1} I_{\alpha_2} I_{\beta_2} + Z_{\alpha_1} Z_{\beta_1} Z_{\alpha_2} Z_{\beta_2})^2 \\ &= \frac{1}{4}(I_{\alpha_1} I_{\beta_1} I_{\alpha_2} I_{\beta_2} - I_{\alpha_1} I_{\beta_1} Z_{\alpha_2} Z_{\beta_2} - Z_{\alpha_1} Z_{\beta_1} I_{\alpha_2} I_{\beta_2} + Z_{\alpha_1} Z_{\beta_1} Z_{\alpha_2} Z_{\beta_2}). \end{aligned} \quad (15)$$

Then, it immediately follows that

$$\begin{aligned} (G^+)^3 &= \frac{1}{16}X_{\alpha_1} X_{\beta_1} X_{\alpha_2} Y_{\beta_2} \cdot (I_{\alpha_1} I_{\beta_1} I_{\alpha_2} I_{\beta_2} - I_{\alpha_1} I_{\beta_1} Z_{\alpha_2} Z_{\beta_2} - Z_{\alpha_1} Z_{\beta_1} I_{\alpha_2} I_{\beta_2} + Z_{\alpha_1} Z_{\beta_1} Z_{\alpha_2} Z_{\beta_2})^2 \\ &= \frac{1}{4}X_{\alpha_1} X_{\beta_1} X_{\alpha_2} Y_{\beta_2} \cdot (I_{\alpha_1} I_{\beta_1} I_{\alpha_2} I_{\beta_2} - I_{\alpha_1} I_{\beta_1} Z_{\alpha_2} Z_{\beta_2} - Z_{\alpha_1} Z_{\beta_1} I_{\alpha_2} I_{\beta_2} + Z_{\alpha_1} Z_{\beta_1} Z_{\alpha_2} Z_{\beta_2}) \\ &= G^+, \end{aligned} \quad (16)$$

thus the ExcitationSolve optimization algorithm is applicable.

B Proof of classical simulability of double excitations acting on the HF state

To prove that the impact of a double excitation on a classical reference state can efficiently be computed, consider the generator of an arbitrary fermionic double excitation

$$G_{pq}^{rs} := i(a_p^\dagger a_q^\dagger a_r a_s - \text{H.c.}), \quad (17)$$

which, under the Jordan-Wigner mapping [55], takes the following form

$$G_{pq}^{rs} \rightarrow \frac{1}{8} \mathcal{Z}_{pq}^{rs} (X_p Y_q Y_r Y_s + Y_p X_q Y_r Y_s - Y_p Y_q X_r Y_s - Y_p Y_q Y_r X_s - Y_p X_q X_r X_s - X_p Y_q X_r X_s + X_p X_q Y_r X_s + X_p X_q X_r Y_s), \quad (18)$$

where the parity string is defined as $\mathcal{Z}_{pq}^{rs} := \prod_{j \in \{p,q,r,s\}} \bigotimes_{k < j} Z_k$. Factoring out any of the $XYYY$ - or $YXXX$ -type odd strings (here we choose $X_p X_q X_r Y_s$), the excitation generators can now be expressed as a product of a Pauli string and some diagonal operator

$$G_{pq}^{rs} = \frac{1}{8} \mathcal{Z}_{pq}^{rs} X_p X_q X_r Y_s (I_p I_q I_r I_s + I_p I_q Z_r Z_s - I_p Z_q I_r Z_s - I_p Z_q Z_r I_s - Z_p I_q I_r Z_s - Z_p I_q Z_r I_s + Z_p Z_q I_r I_s + Z_p Z_q Z_r Z_s). \quad (19)$$

This product decomposition is specifically designed such that the $XXXY$ string commutes with the remaining Z -terms. This would not be the case if one were to factor out an even string, e.g., $XXYY$. Now consider the application of the double excitation to the reference state where the orbitals (p, q) are occupied and (r, s) are unoccupied:

$$U_{pq}^{rs}(\theta) |\psi_0\rangle = \exp(-i\theta G_{pq}^{rs}) |\psi_0\rangle = \exp(\mp i\theta X_p X_q X_r Y_s) |\psi_0\rangle. \quad (20)$$

Exploiting the eigenvalue relation of all Z -terms w.r.t. $|\psi_0\rangle$ cancels out the pre-factor of 1/8, and introduces a phase-flip based on the parity of $|\psi_0\rangle$ w.r.t. to the orbitals affected by the parity-string \mathcal{Z}_{pq}^{rs} . The action of the double excitation has therefore been reduced to a single Pauli rotation instead of eight. This can serve as a helpful circuit optimization technique for the first few excitations as it has been demonstrated in Ref. [16]. Using the Euler formula, one may now express the resulting state as

$$|\psi(\theta)\rangle = \cos(\theta) |\psi_0\rangle \pm \sin(\theta) |\psi_1\rangle, \quad (21)$$

where $|\psi_1\rangle$ differs from $|\psi_0\rangle$ in that the orbitals (p, q) are unoccupied and (r, s) are occupied. We may now compute the energy impact

$$\begin{aligned} \Delta E(\theta) &= \langle \psi_0 | H | \psi_0 \rangle - \langle \psi(\theta) | H | \psi(\theta) \rangle \\ &= \frac{1 - \cos(2\theta)}{2} [\langle \psi_0 | H | \psi_0 \rangle - \langle \psi_1 | H | \psi_1 \rangle] \mp \frac{\sin(2\theta)}{2} [\langle \psi_0 | H | \psi_1 \rangle + \langle \psi_1 | H | \psi_0 \rangle] \\ &= \frac{(1 - \cos(2\theta))}{2} (h_{pp} + h_{qq} - h_{rr} - h_{ss}) + \frac{\sin(2\theta)}{2} \Re\{h_{pqrs}\}. \end{aligned} \quad (22)$$

In the last step, we inserted the matrix elements of the electronic structure Hamiltonian (assuming that the quartic terms are defined with a prefactor of 1/2). The prefactor due to the parity cancels out in the last step. In the following, it is convenient to employ the identity $a \sin(x) - b \cos(x) = R \sin(x + \varphi)$ with $R = \sqrt{a^2 + b^2}$ and $\varphi = \arctan(b/a)$. With this, we can immediately infer that the maximum energy impact is given by

$$\Delta E := \Delta E(\theta_{\max}) = \frac{1}{2} \left(h_{pp} + h_{qq} - h_{rr} - h_{ss} + \sqrt{(h_{pp} + h_{qq} - h_{rr} - h_{ss})^2 + \Re\{h_{pqrs}\}^2} \right), \quad (23)$$

with the optimal angle

$$\theta_{\max} = \frac{\pi}{4} - \frac{1}{2} \arctan \left(\frac{h_{pp} + h_{qq} - h_{rr} - h_{ss}}{\Re\{h_{pqrs}\}} \right). \quad (24)$$

This way, the impact of any double excitation on the Hartree-Fock ground state can be efficiently computed.

If the initial state is obtained from Kohn-Sham theory, as observed in UCC-based post-DFT calculations [34, 35], single excitations can potentially lower the energy compared to the reference state. In that case the same technique can be applied to reduce the single excitations to simple XY -rotations. In addition, one can then compute the energy impact according to

$$\Delta E = \frac{1}{2} \left(h_{pp} - h_{qq} + \sqrt{(h_{pp} - h_{qq})^2 + \Re\{h_{pq}\}^2} \right), \quad (25)$$

$$\theta_{\max.} = \frac{\pi}{4} - \frac{1}{2} \arctan \left(\frac{h_{pp} - h_{qq}}{\Re\{h_{pq}\}} \right). \quad (26)$$

C Operator selection for other bondlengths

We find that for molecules in a linear alignment such as the LiH molecule the same operators are selected by ES for all bondlengths. In Figure 7 we plot, which operator is selected at different bondlengths for the LiH and H₂O molecules, black meaning that the operator is chosen, white that it is not. Without going into detail which operators are the relevant ones, it becomes apparent, that for LiH the bondlength does not play a role for the selection. For H₂O on the other hand the selected operators vary with the bondlength. The reason is that in linear molecules even as the bond is stretched or compressed, the same orbitals are overlapping and so the same excitations are relevant. In a molecule such as H₂O on the other hand with a bond angle of 104.5° the overlap between orbitals changes and so also the operator selection is dependent on the bondlength. However even in H₂O many similar bondlengths select similar operators. Therefore if we want to know the relevant operators at multiple bondlengths it may only be necessary to determine them once (for linear molecules) or a few times (for non-linear molecules) and interpolate the rest saving further computational power.

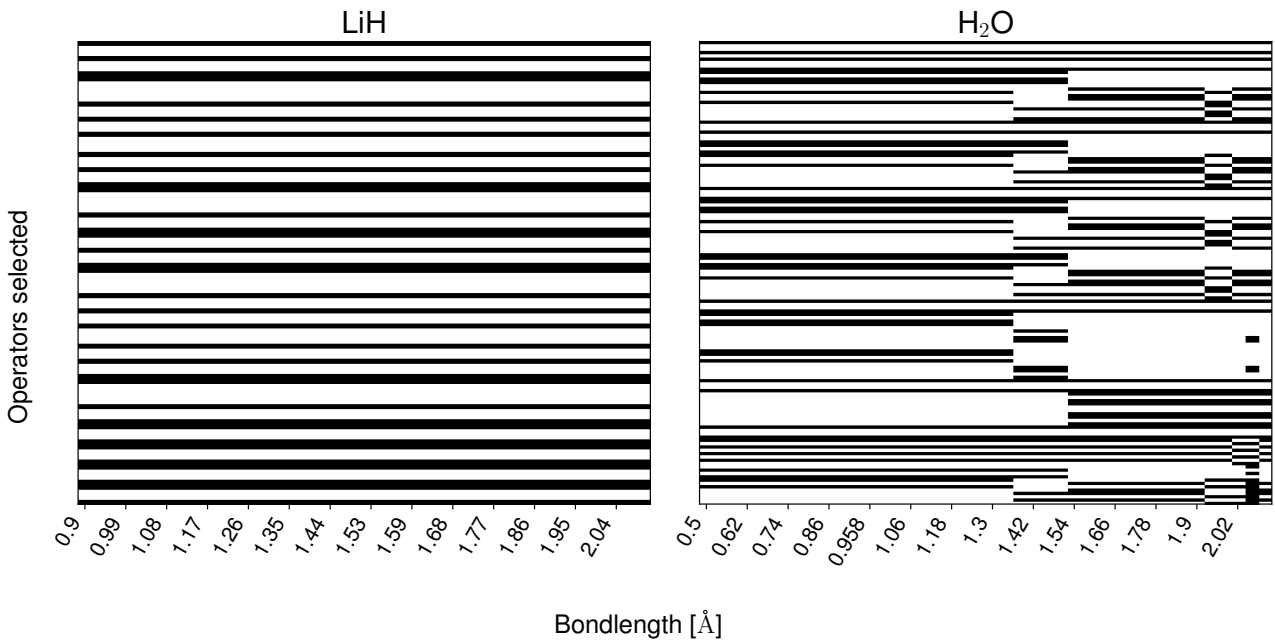


Figure 7: Operator selection for LiH and H₂O using ExcitationSolve and ES. Operators marked black are selected for that bondlength, operators marked in white are not relevant. The y-axis shows all the operators in the operator pool.